Research Article Vol. 13, No. 6 / 1 Jun 2023 / Optical Materials Express 1808
Optical Materials EXPRESS

Optical and electrical properties characterisation of photovoltaic spatial-light modulators

NICOLAS BROUCKAERT,[1,*] DENITSA BANKOVA,[1] THOMAS HEISER,[2] GIAMPAOLO D'ALESSANDRO,[3] AND MALGOSIA KACZMAREK[1]

[1]School of Physics and Astronomy, Southampton S017 1BJ, United Kingdom
[2]ICube Research Institute, Université de Strasbourg, Centre National de la Recherche Scientifique, Strasbourg Cedex 2 67037, France
[3]School of Mathematics, Southampton S017 1BJ, United Kingdom
[*]nb1f20@soton.ac.uk

Abstract: Liquid crystal photovoltaic spatial-light modulators use photovoltaic layers as an integrated power source to switch from a transparent to an opaque state depending on the ambient illumination. We use non-invasive cross-polarised intensity measurements, to fit photovoltaic parameters, namely photo-generated voltage and photoconductivity, in a sealed device and map their variation across its surface. This methodology was used to estimate the effect of light intensity on these devices and to monitor changes of the photovoltaic parameters over a nine-month period.

© 2023 Optica Publishing Group under the terms of the Optica Open Access Publishing Agreement

1. Introduction

Liquid crystal devices, with their ability to change and control the light phase upon the application of an electric or a magnetic field, are widely used in various applications such as displays, variable wave-plates or light modulators [1–3]. In spatial-light modulators, the liquid crystal properties are harnessed to control light transversally to the propagation direction, e.g., as in optical tweezers or beam shaping devices [4–6]. Due to low operating voltage, typically up to 2 volts, this technology is a good candidate for green energy and for being powered through an integrated organic solar cell. By combining a transparent high voltage solar cell and a low operating voltage liquid crystal (LC), we can in principle obtain a self-powered modulator that is able to switch automatically from its transparent to its opaque state without any external input other than external illumination. The transparent state could be recovered either by disconnecting the device's electrodes or by taking off the illumination source (Fig. 1). Such devices are thus suitable for applications such as photosensors, optical limiters and wavelengths filters. The use of photoactive substrates was explored theoretically [7] and demonstrated with crystalline Ce:SBN [8] and CdTe [9] substrates using a beam coupling setup for recording of phase grating in LC layers. Similar technologies also use photoconductive substrates to spatially modulate the liquid crystal alignment [10–12], however, in these systems it is essential to use an external power source, exploit the photoconductive properties of the layers as well as ensure spatially periodic light modulation to induce local changes in the LC alignment. Instead, in the system presented here, the combination of the LC layer with a solar cell, can induce a localised modulation of the LC alignment using a single homogeneous light source, ultimately without the need of an external power source. This technology, called Photovoltaic Spatial-Light Modulators (Photovoltaic SLM, or PSLM) has been demonstrated using low threshold voltage liquid crystals and single or tandem organic photovoltaic units (PVUs) but with their top metallic electrode replaced by a transparent conductive polymer to ensure transparency of the device [13]. The photovoltaic

#491603 https://doi.org/10.1364/OME.491603
Journal © 2023 Received 31 Mar 2023; revised 5 May 2023; accepted 20 May 2023; published 1 Jun 2023

Optical Materials EXPRESS

part can, in principle, consist of either organic photovoltaic materials, perovskite or an inorganic semiconductor layer. An organic photovoltaic layer, despite lower conversion efficiency, offers several benefits: it is relatively easy to deposit and to integrate within a single device. The voltage required has to be higher than the voltage threshold, but no significant current is needed. Furthermore, having an organic photovoltaic layer gives a high degree of flexibility in the choice of absorption wavelength range and, hence, transparency window [14–16]. Finally, the layer can be mechanically rubbed and thus serve a dual purpose, acting as an alignment layer as well. In summary, organic photovoltaic layers make the PSLM, widely tuneable and adaptable [17,18].

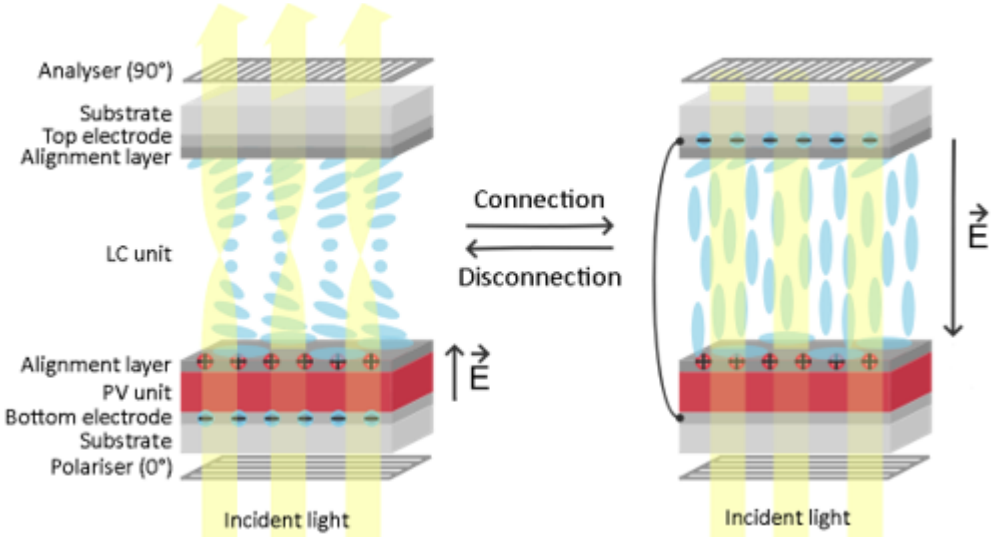

Fig. 1. Schematic of a PSLM structure and response upon illumination when disconnected (left) and connected (right). When the electrodes are disconnected, the PSLM is in its off-state and transmits the light through. Connected electrodes lead to a delocalisation of the negative charges from the bottom electrode to the top one. Thus, the photo-generated electric field, initially present across the PVU is now applied to the LC unit, reorienting the LC molecules, and blocking the polarised light leading to the on-state. In the case of a local illumination, the responding area will be defined by the ability of the positive charges to diffuse and migrate along the PVU unit and the bottom alignment layer, meaning that the resolution of the device can be tuned with its conductivity.

However, in PSLMs, the interface effects are important, and it is not trivial to predict the LC response when in contact with a photosensitive multi-layer structure such as an organic solar cell. In this paper, we will present an optical method to study liquid crystal properties in PSLMs and the photovoltaic characteristics of the integrated PVU. We will first detail the measurement method and the model used to fit the PSLM parameters. The bulk of the paper is the Results section, where we present and analyse all our experimental results to extract pretilts, photovoltage of PSLMs and estimate the photoconductivity of our PVUs. Possible extensions of this work to measure other PSLM parameters are discussed in the conclusions.

2. Materials and methods

Here we focus on the optical methodology to measure PSLM parameters. Our main tool is the Optical Multi-Parameters Analyser (OMPA), used to extract liquid crystal [19–23] and PVU characteristics from cross-polarised intensity measurements. Detailed descriptions of the

Optical Materials EXPRESS

fabrication of the PVUs and of the assembly of PSLMs are provided in the supporting information [24,25]

2.1. Cross-polarised intensity measurements

Measurements were performed using a standard cross-polarised intensity (CPI) setup that includes an additional CCD camera for wide area measurements. This setup is presented in Fig. 2, and can be used to study the phase shift in the wave fronts induced by liquid crystal devices, such as LC wave plates or phase SLMs, by measuring the modulation of the amplitude of the light going through the whole setup when applying an increasing voltage to the cell. The basic CPI setup consists of two crossed polarisers (polariser and analyser) with a planar liquid crystal cell placed in between them. With no applied voltage the LC director is aligned at an angle of 45° with respect to both polariser axes. The light source used is a laser beam with a wavelength of 532 nm and a power of 4.5 mW.

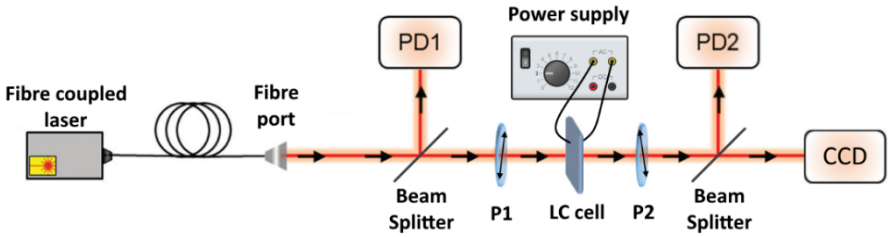

Fig. 2. Schematic of CPI setup used by the OMPA. An incident laser beam is split in two beams by a beam splitter. One is directed to a first photodetector PD1 (reference signal), and the second continues and goes through the first polariser P1, the studied LC cell and a second crossed polariser P2 (analyser). Then, the output is recorded either by another photodetector for small area scanning, or by a CCD camera to record a large area response. When using the CCD camera to record large areas, two lenses, placed after the fibre port, expand the beam. The setup is kept enclosed to avoid any external, unwanted sources of illumination or background noise.

In single spot measurements, the illuminated cell area is about 6mm^2. Two beam splitters redirecting parts of the incident light are placed before the first polariser and after the analyser to extract a reference and an output signal respectively through two photodetectors (PD1 and PD2 respectively) as a function of the voltage applied to the cell. The end result of this measurement is a single CPI trace that is fitted to extract the PSLM parameters.

In wide area measurements, instead, the beam is expanded and collimated so that it illuminates the entire PSLM surface area (~150mm^2). In this configuration, a CCD camera is used to record the cell response over its entire surface [19,21]. An algorithm then selects the area of the sample with the highest signal to noise ratio and divides it in an 8×8 grid to produce 64 CPI traces that are then fitted to extract local properties and create cell maps.

The setup is driven by a software which performs both data acquisition and analysis [19–21]. The studied cells were addressed with a sinusoidal AC signal with a 10kHz frequency, with a signal amplitude varying from 0 to 10 V with steps of 0.02 V. The average value of the CPI is recorded for each voltage step. The CPI obtained is then normalised to obtain a curve with minimum and maximum values of 0 and 1 respectively.

Filters of different optical densities (OD) can be added to the setup to change the intensity of the laser beam, and thus the cell illumination. The filters used in this study go from an optical density of 3 (OD3) to 0 (OD0) corresponding to light transmission from 0.1% to 100% respectively. Two types of PVU active layers were studied, PBDB-T-2F (PM6) or poly(3-hexylthiophene) (P3HT) blended with indene-C60 (ICBA). In OD0 conditions, the PM6 and P3HT-based PVUs

Optical Materials EXPRESS

are expected to produce a photovoltage output at 532 nm [26,27]. The laser intensity at the sample position (after the first polariser) in OD0 conditions was measured to be 370W/m^2.

2.2. Model and fitting procedure

The OMPA built-in algorithms and the underlying model were reported previously [19–23] and used to extract critical LC parameters such as rotational viscosity, elastic constants, cell thickness, pretilt angle and polar anchoring energy of any planar liquid crystal devices using standard (polyimide) or photoconductive (poly-vinylcarbazole) alignment layers, allowing a quick, reliable and easy method to extract LC characteristics. The correct fitting procedure requires the input of some intrinsic parameters, namely the dielectric constants and the refractive indices (or birefringence [28]) of the liquid crystals used.

In the core model, detailed in [21] and summarised in the supporting information [24,25], an assumption was made regarding the alignment layer, modelled as a standard polyimide (PI) layer a few nanometres in thickness. It was neglected with respect to that of the much thicker liquid crystal layer. In the case of PSLMs, the alignment layer sits on top or is part of a multilayer photovoltaic structure. The total thickness of these stacked layers is typically larger than 100 nm so that their total impedance can no longer be considered negligible compared to that of the liquid crystal layer. It is also important to take into consideration that some of these layers are photoactive. Therefore, it is expected that some of their properties, such as their conductivity, will change upon illumination [29]. The OMPA model for PSLMs presented here, referred to in this study as photoOMPA, represents all these stacked layers as a combined single impedance whose parameters can be determined by fitting the CPI trace.

In the absence of photovoltaic effects, the voltage across the liquid crystal layer V_{LC}, can be estimated by representing the liquid crystal device as a potential divider with two impedances, one representing the alignment layer (Z_{AL}) and the second one the LC layer (Z_{LC}). The voltage dropped across the liquid crystal layer (V_{LC}) can then be written as:

$$V_{LC} = V_{in}\frac{Z_{LC}}{Z_{LC} + Z_{AL}}\,, \tag{1}$$

where Z_{AL} is small with respect to Z_{LC}, and V_{in} is the input AC voltage.

In the regime of operation of the PSLMs it is possible to represent the PVU with a simplified circuit consisting of a DC photovoltage generator with its own internal capacitance C_{PV} and a light intensity dependent series resistance R_{PV}. The equivalent circuit is presented in Fig. 3. In this circuit there are two voltage sources applied to the LC layer, a DC voltage (V_{PV}) generated by the PVU, and the externally applied AC voltage (V_{in}). The DC voltage across the liquid crystal layer is given by Eq. (1), with the impedances replaced by the corresponding resistances, R_{LC} and R_{PV} for the liquid crystal and PVU layers respectively,

$$V_{LC\,(DC)} = V_{PV}\frac{R_{LC}}{R_{LC} + R_{PV}}\,. \tag{2}$$

The AC voltage amplitude, $V_{LC\,(AC)}$, is also given by Eq. (1), with Z_{AL} becoming Z_{PV}, the PVU impedance.

The total voltage applied to the LC layer is the sum of the DC and AC component,

$$V_{LC\,(total)} = V_{LC\,(DC)} + V_{LC\,(AC)}\cos(\omega t)\,, \tag{3}$$

where ω is the AC angular frequency. Finally, the effective voltage ($V_{LC\,(eff)}$) seen by the liquid crystal molecules is the time mean square average of the total applied voltage,

$$V_{LC\,(eff)} = \sqrt{(V_{LC\,(DC)})^2 + \frac{(V_{LC\,(AC)})^2}{2}}\,. \tag{4}$$

Optical Materials EXPRESS

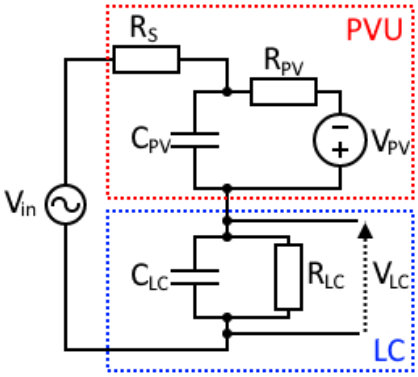

Fig. 3. Schematic of the equivalent circuit of a PSLM. The circuit is divided into two main components, the PVU and the LC layer. R_S is the internal series resistance of the PVU, which can be neglected regarding to the larger R_{PV} corresponding to the shunt resistance of the PVU. The capacitances of the PVU and the LC layers are represented as two capacitors named C_{PV} and C_{LC} respectively.

By measuring the LC characteristics at a very low light intensity, to nullify the photogenerated voltage (PV) contribution, it is possible to get a reference CPI measurement that is free of any DC component. Then, by measuring the CPI at higher light intensities, the PV contribution for different light intensities, with respect to the reference CPI, can be extracted. Alternatively, the reference CPI measurement can be carried out at a wavelength where the PVU is fully transparent and will not generate any photovoltage.

The model was validated through measurements of reference cells with known photovoltaic properties. Reference PVUs were first built following the method described in the supplementary information, and fully characterised through I-V curves using a solar simulator under an illumination of 1sun. To do so, PVUs are exposed to a high intensity light, corresponding to the average intensity and spectrum of the sun light on earth, and increasing voltages are applied to the cell, while the resultant current is recorded. On solar cell I-V curves, the additional voltage applied needed to cancel any current flow in the PVU under illumination is called the open circuit voltage (V_{OC}), which is close to the maximum photovoltage that the PVUs will be able to provide. After determining the V_{OC} of our PVUs, PSLMs were assembled, and corresponding CPI measurements were carried out at high light intensity to compare the fitted photovoltage to the V_{OC} values obtained previously. An example is provided in the supporting information (Fig. S1): from this we see that the agreement between the two methods is excellent, as both give the same photovoltage (440 mV) within experimental error.

3. Results and discussion

In this section, we present the effects of the photovoltaic layers on the LC response upon illumination. We then present measurements of the liquid crystal and photovoltaic layer parameters. The ability to record the aging of PSLMs will also be shown in terms of evolution of the PVU efficiency. Finally, we will introduce a method to map all these properties across a wide PSLM area to detect defects in the PVU layer.

3.1. Effects of a light intensity on PSLM response

When exposed to light at a wavelength absorbed by the photovoltaic layer, the PSLMs produce an electric field [26] which is applied across the liquid crystal (Fig. 1). As a CPI transmission curve shows the light transmission of a cell across a range of applied voltages, the addition of a

Optical Materials EXPRESS

fixed DC voltage is expected to produce a shift of the CPI following Eq. (4). This effect is shown on Fig. 4, where two PM6:ICBA PSLMs with different LCs are exposed to a 532 nm laser at full light intensity (OD0, blue lines) and at a strongly attenuated close to zero light intensity (OD3, red lines). The samples were not moved between the measurements to ensure that the illuminating beams were at the same spot on the PSLMs.

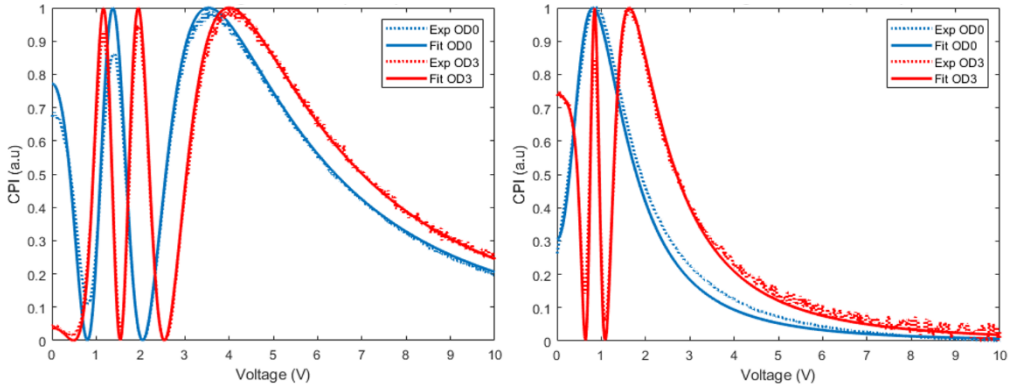

Fig. 4. CPI measurements (dotted lines) and corresponding fits (solid lines) at 532 nm of PM6:ICBA PSLMs filled with E7 (left) and QYTN (right). Measurements were performed using two filters of different optical densities, OD0 in blue and OD3 in red. The use of an OD3 filter (red) can be approximated as having a cell in the dark as the photogenerated current is negligeable due to the extremely low light intensity.

It is noticeable that the effect of increasing light intensity is not just a straightforward shift of the CPI curves. Their shape is also altered because of changes of some PVU properties upon illumination. For example, when exposed to wavelengths absorbed by the photovoltaic layers, the conductivity of the PVU is expected to increase [29] thus lowering the voltage dropped across the PVU. The impact of this change depends on the PVU total thickness, and for such thin films, the dark conductivity depends strongly on charge carrier diffusion from the interfaces [30], so small changes in its uniformity can lead to different conductivity results. Hence, an accurate estimate of this PVU thickness and interface properties opens the possibility to also estimate the PVU conductivity from CPI measurements. In this study, the total PVU thickness was estimated to be 120 nm from the measurement of a reference cell built in the same conditions. The effect of different PVU conductivities on CPI simulations is shown on Fig. 5, indicating that the effect is small, but measurable at least in a range of PVU conductivities, 0.5 to 5 µS/m in the case of Fig. 5.

3.2. *Extraction of liquid crystal and photovoltaic properties*

The photoOMPA algorithm fits an experimental CPI to find the best parameter combination that will match the experimental curve [19–21]. The addition of light dependent parameters from the PVU (conductivity, photovoltage) makes the fitting procedure more complex and may reduce the precision of the fitted parameters. To minimise this effect, measurements were first performed in the dark (OD3) to extract the intrinsic LC parameters that would remain constant with different light intensities, namely the elastic constants and the LC layer thickness. Measurements in OD3 conditions can also give starting values of parameters that may change when the PVU is exposed to light, such as the pretilt or the anchoring energy. The errors on the pretilt and photovoltage increase with light intensity due to the progressive shift and disappearance of peaks to fit. However, these errors are estimated to remain below 5% from multiple fittings.

Optical Materials EXPRESS

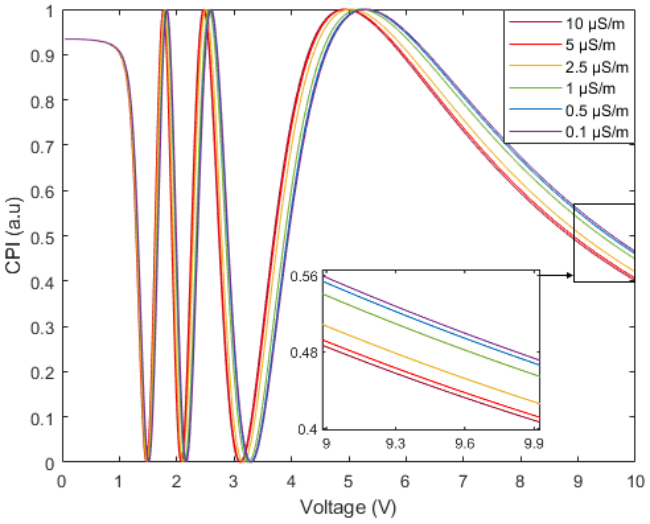

Fig. 5. Simulated CPIs of a PSLM with a 120 nm thick PVU layer with different conductivities at 532 nm. The LC used is E7 with fixed parameters from the literature [19]: $K_1 = 10.9$pN, $K_3 = 17.895$pN, $\varepsilon_{//} = 19.54$, $\varepsilon_{\perp} = 5.17$, $n_e = 1.7558$, $n_o = 1.5282$, cell thickness = 8µm, pretilt = 2°. No photovoltage is simulated.

Pretilt (θ) and photovoltage (V_{PV}) fitted values of P3HT:ICBA and PM6:ICBA based PSLMs using both E7 and QYTN-004 (QYTN) liquid crystals are reported in Table **1** for different light intensities, and a summary of their evolution is plotted in Fig. 6. The corresponding CPI traces for OD0 and OD3 conditions are available in Fig. S2.

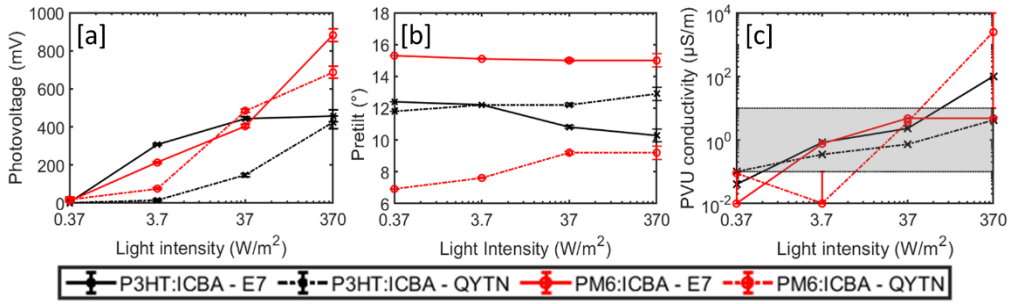

Fig. 6. Evolution of the photovoltage (a) and the pretilt (b) as a function of light intensity at 532 nm for the different structures. A light intensity of 370W/m^2 corresponds to using an OD0 filter. The evolution of the estimated photoconductivity of the PVU is shown in block (c) for different light intensities and a fixed PVU thickness of 120 nm. Only measurements that are in the shaded area are sufficiently accurate to detect a trend for the estimated PVU thickness. Lines are a help to the eyes.

We can observe from Fig. 4 and Table 1 that the photoOMPA is able to produce a good fit of the experimental traces, despite the deviation between the experimental and fitted curves observed near the extrema, especially at low voltages. This is due to the experimental data not having normalised maximums and minimums with fixed height of 1 and 0 respectively, as expected by the model. One possible origin of this phenomenon are inhomogeneities in the cell layers that affect the light transmission at low voltages. These disappear at higher applied AC voltages as the DC contribution gets smaller. The laser spot size is 6mm^2, and the photovoltaic properties or

Optical Materials EXPRESS

Table 1. Evolution of the average fitted photovoltage and pretilt upon illumination for different PSLM structures and light intensities

	P3HT:ICBA (E7)		P3HT:ICBA (QYTN)		PM6:ICBA (E7)		PM6:ICBA (QYTN)	
Filter used	θ (°)	V_{PV} (mV)	θ (°)	V_{PV} (mV)	θ (°)	V_{PV} (mV)	θ (°)	V_{PV} (mV)
OD3	12.4	5	11.8	0	15.3	10	6.9	20
OD2	12.1	310	12.2	15	15.1	215	7.6	75
OD1	10.8	445	12.2	145	15.0	405	9.2	485
OD0	10.3	460	12.9	425	15.0	880	9.2	685

alignment quality of the LC can slightly vary over the studied area. The photodetector averages the local response, and this can lead to extrema which are not a perfect maximum or minimum. A visualisation of this phenomenon is illustrated with camera recordings in Fig. S3 where cell inhomogeneities at low applied voltage can be observed.

The fitted photovoltages generated for different light intensities show an increase of the photovoltage with light intensity, as expected (see Fig. 6(a)), with a higher maximum output for PM6:ICBA based PSLMs (880 and 685 mV with E7 and QYTN respectively) compared to the P3HT:ICBA ones (460 and 425 mV with E7 and QYTN respectively). The fitted pretilts do not show a specific trend and can be considered light intensity independent (see Fig. 6(b)). It is noticeable that the pretilt angles are large (7° to 15°). This may be due to the nature of the alignment layer, that uses the directionality of the P3HT side chains to orient the LC molecules. As these side chains have an angle with the surface, they may lead to a higher pretilt as compared to an alignment method that uses microgrooves and typically gives pretilt angles of up to a few degrees [31,32]. An estimate of the PVU photoconductivity at different light intensities is also shown, as a guide, in Fig. 6(c), which indicates an upward trend of the conductivity with light intensity, as expected. These data, however, should be treated with caution as it may be affected by systematic errors due to the limited accuracy of the PVU layer thickness estimate. Moreover, as shown in Fig. 5, only conductivities in the grey band can be reasonably fitted from CPI measurements.

3.3. Monitoring PSLM aging

The main advantage of the photoOMPA optical method is its ability to capture photovoltaic properties of a PVU, even when integrated in a closed system and thus without direct, external contact with the PVU boundaries for a direct measurement. An important aspect for devices that include organic solar cells is their stability over time [33–35]. The characterisation through the photoOMPA non-invasive method allows us to monitor both the LC and PVU properties and follow the evolution of critical parameters such as pretilt and photovoltage with time and usage. Such measurements were carried out on the PM6:ICBA based PSLMs presented in the previous section. The samples were encapsulated and stored in a closed and opaque shelf, in air, for 9 months. The evolution of their response for different light intensities after 9 months has been studied and is summarised in Fig. 7 and Table **2**. The corresponding CPI traces are in Fig. S2.

The trend is the same for both cells: the voltage shift gets smaller with time. Namely, the photovoltage drops by approximately 70% over 9 months for the PSLM filled with LC E7, and 27.5% for the one filled with LC QYTN. It is also noticeable that the pretilt of the PM6:ICBA based PSLM filled with E7 changed from 15° to 11°. This shows that both the alignment layer and PVU properties do not maintain their original parameters over nine months in a PSLM configuration. These changes could be due to either a degradation of the photovoltaic materials or of the P3HT-LC interface (e.g., partial dissolution, mechanical change of the pretilt due to the

Optical Materials EXPRESS

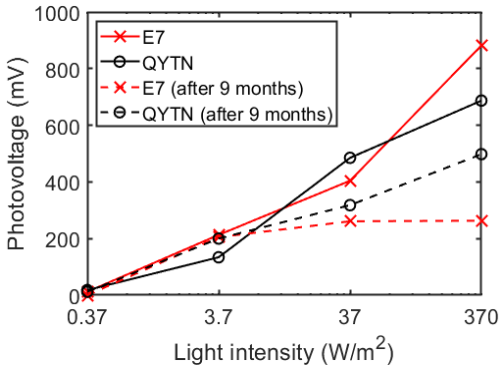

Fig. 7. Evolution of the fitted photovoltages at different light intensities for PM6:ICBA PSLMs immediately after assembling (solid lines) and after 9 months (dashed lines). A light intensity of 370W/m^2 corresponds to the OD0 condition. Lines are a guide for the eyes.

Table 2. Evolution of the average fitted photovoltage and pretilt upon illumination for PM6:ICBA PSLMs after 9 months at different light intensities

	PM6:ICBA (E7)		PM6:ICBA (E7) after 9 months		PM6:ICBA (QYTN)		PM6:ICBA (QYTN) after 9 months	
Filter used	θ (°)	V_{PV} (mV)	θ (°)	V_{PV} (mV)	θ (°)	V_{PV} (mV)	θ (°)	V_{PV} (mV)
OD3	15.3	10	11.0	0	6.7	20	9.1	10
OD2	15.1	215	11.1	205	7.1	135	9.0	200
OD1	15.0	405	11.2	260	9.2	485	9.1	320
OD0	15.0	880	11.0	265	9.2	685	8.8	500

aging). We are currently studying these mechanisms, in particular how different nematic LCs contribute to the aging of the PVUs.

3.4. *Discussion about the mapping of PSLM properties*

One of the advantages of using an optical method to characterise the PSLM's photovoltaic properties, is the option to either probe a small cell area by using a narrow beam, or to expand the beam to uniformly illuminate the whole PSLM and record spatially varying responses using a CCD camera. While the previous results were focused on the use of a narrow beam, this section will demonstrate the potential of the expanded beam method to map the photovoltaic properties of the PSLM and detect potential defects across the PVU surface.

Expanded beam measurements were carried out using the PM6:ICBA PSLMs nine months after assembly. The results are shown in Fig. 8 for an area of 12.25mm^2 (3.5 mm x 3.5 mm). The PSLM filled with QYTN (left) shows a homogeneous distribution of the photovoltage, whereas the PSLM filled with E7 (right) shows a defect in its central part that corresponds to a non-productive section of its PVU. The average photovoltages computed from these images are 242 mV and 521 mV for the E7 the QYTN PSLM, respectively. These values are in close agreement with the ones presented in Table 2 where a focused laser beam was used.

More in-depth analysis of the aging and the stability of PSLMs is ongoing but this preliminary analysis shows that even after months of storage, the aging of the PVU does not cause the formation of large area defects that would decrease the average voltage across the entire PSLM.

The possibility of mapping PVU and LC parameters across the cell surface opens up the possibility of in-depth studies of PSLMs, apart from the effect of aging. For example, maps of the

Optical Materials EXPRESS

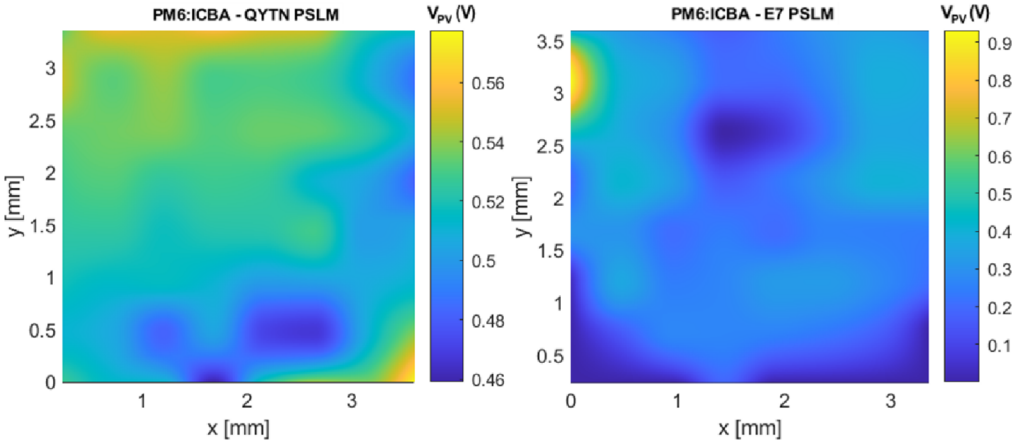

Fig. 8. 2D map of the photo-generated voltage across the PSLM on a 3.5 mm x 3.5 mm area for two PM6:ICBA PSLMs, taken 9 months after assembling. The PSLM filled with E7 (right) shows a defect with a non-productive zone in the middle, and an artefact in the top left corner which is due to a poor-quality CPI that did not allow a good fit in this specific region. It is crucial, in term of resolution, to keep in mind that on the 3.5 mm x 3.5 mm area, the grid system spaced the measurements (and thus, fits) by 0.5 mm (see 2.1).

conductivity of the photovoltaic layers should enable the detection of potential structural defects in the PVU layer. However, to reach this goal, a corresponding mapping of the photovoltaic layers thickness would be required as these parameters are strongly interdependent. Similarly, photovoltage maps offer a measure of the spatial resolution of the PSLM at least on the scale of a fraction of a millimetre.

4. Conclusion

We successfully demonstrated a method to extract both the photovoltaic and the liquid crystal parameters from an enclosed photovoltaic spatial-light modulator using an optical cross-polarised intensity measurement. If the values of the liquid crystal refractive indices and the dielectric coefficients are known and the photovoltaic layer thickness determined, the photoOMPA can provide critical parameters for the efficient operation of a modulator, such as elastic constants, LC thickness, pretilt or anchoring energy. It provides a reliable estimate of the photovoltage generated by an integrated organic photovoltaic unit, as well as its conductivity. This method can be used either to probe specific regions of the device or expanded to study a large area of the sample to determine how homogeneous is the response of the PSLM. With a precise measurement of the PVU thickness across the area, mapping of the PVU conductivity could also be carried out to monitor for any changes in the decrease of the PVU efficiency over time.

Funding. Agence Nationale de la Recherche (ANR-19-CE05-0036).

Acknowledgments. The authors would like to thank Dr. N. Podoliak, Dr. S. Fall, Dr. Y. Lin, Prof. O. Hovorka and Prof. J-F. Black for their help and contribution to the project and data acquisition.

Disclosures. The authors declare no conflict of interest.

Data availability. Data underlying the results presented in this paper are available in Ref. [36].

Supplemental document. See Supplement 1 for supporting content.

Optical Materials EXPRESS

References

1. Y. Shen and I. Dierking, "Perspectives in liquid-crystal-aided nanotechnology and nanoscience," Appl. Sci. **9**(12), 2512 (2019).
2. M. Munna, F. Anwar, and R. A. Coutu Jr, "Nematic Liquid Crystal Composite Materials for DC and RF Switching," Technologies **7**(2), 32 (2019).
3. A. Kumar, D. P. Singh, and G. Singh, "Recent progress and future perspectives on carbon-nanomaterial-dispersed liquid crystal composites," J. Phys. D: Appl. Phys. **55**(8), 083002 (2022).
4. R. Li and L. Cao, "Progress in Phase Calibration for Liquid Crystal Spatial Light Modulators," Appl. Sci. **9**(10), 2012 (2019).
5. U. Effron, S. T. Wu, and T. D. Bates, "Nematic liquid crystals for spatial light modulators: recent studies," J. Opt. Soc. Am. B **3**(2), 247 (1986).
6. K. M. Johnson, D. J. McKnight, and I. Underwood, "Smart Spatial Light Modulators Using Liquid Crystals on Silicon," IEEE J. Quantum Electron. **29**(2), 699–714 (1993).
7. N. V. Tabiryan and C. Umeton, "Surface-activated photorefractivity and electro-optic phenomena in liquid crystals," J. Opt. Soc. Am. B **15**(7), 1912–1917 (1998).
8. G. Cook, C. A. Wyres, M. J. Deer, and D. C. Jones, "Hybrid Organic-Inorganic Photorefractives," Liquid Crystals VII. **5213**, 63 (2004).
9. J. Gvozdovskyy, K. Shcherbin, D. R. Evans, and G. Cook, "Infrared sensitive liquid crystal photorefractive hybrid cell with semiconductor substrates," Appl. Phys. B **104**(4), 883–886 (2011).
10. U. Bortolozzo, S. Residori, and J. P. Huignard, "Beam coupling in photorefractive liquid crystal light valves," J. Phys. D: Appl. Phys. **41**(22), 224007 (2008).
11. K. Shcherbin, I. Gvozdovskyy, A. Shumelyuk, J. Slagle, and D. R. Evans, "Near-infrared sensitive two-wave mixing adaptive interferometer based on a liquid crystal light valve with a semiconductor substrate," Appl. Opt. **61**(22), 6498 (2022).
12. M. Kaczmarek and A. Dyadyusha, "Structured, photosensitive PVK and PVCN polymer layers for control of liquid crystal alignment," J. Nonlinear Optic. Phys. Mat. **12**(04), 547–555 (2003).
13. S. Fall, J. Wang, T. Regrettier, N . Brouckaert, O. A. Ibraikulov, N. Leclerc, Y. Lin, M. I. Elhaj, L. Komitov, P. Lévêque, Y. Zhong, M. Brinkmann, M. Kaczmarek, and T. Heiser, "Self-Powered Dynamic Glazing Based on Nematic Liquid Crystals and Organic Photovoltaic Layers for Smart Window Applications," ACS Appl. Mater. Interfaces **15**(3), 4267–4274 (2023).
14. S. Shafian, J. Son, Y. Kim, J. K. Hyum, and K. Kim, "Active-Material-Independent Color-Tunable Semi-transparent Organic Solar Cells," ACS Appl. Mater. Interfaces **11**(21), 18887–18895 (2019).
15. Y. Cui, C. Yang, H. Yao, J. Zhu, Y. Wang, G. Jia, F. Gao, and J. Hou, "Efficient Semi-transparent Organic Solar Cells with Tunable Color enabled by an Ultralow-Bandgap Nonfullerene Acceptor," Adv. Mater. **29**(43), 1703080 (2017).
16. H. Meddeb, M. Götz-Köhler, N. Neugebohrn, U. Banik, N. Osterthun, O. Sergeev, D. Berends, C. Lattyak, K. Gehrke, and M. Vehse, "Tunable photovoltaics: adapting solar cell technologies to versatile applications," Adv. Energy Mater. **12**(28), 2200713 (2022).
17. H. S. Shin, R. Manda, T. H. Kim, J. G. Park, Y. J. Lim, B. K. Kim, Y. H. Lee, and S. H. Lee, "Multi-layered carbon nanotube UV polariser for photo-alignment of liquid crystals," Liquid Crystals **47**(11), 1604–1611 (2020).
18. J. P. Auton and M. C. Hutley, "Grid polarisers for use in the near infrared," Infrared Phys. **12**(2), 95–100 (1972).
19. E. Perivolari, G. D'Alessandro, V. Apostolopoulos, N. Brouckaert, T. Heiser, and M. Kaczmarek, "Two-dimensional snapshot measurement of surface variation of anchoring in liquid crystal cells," Liq. Cryst. **48**(15), 2086–2096 (2021).
20. T.P. Bennett, M.B. Proctor, M. Kaczmarek, and G. D'Alessandro, "Lifting degeneracy in nematic liquid crystal viscosities with a single optical measurement," J. Colloid Interface Sci. **497**, 201–206 ISSN 0021-9797 (2017).
21. T. Bennett, M. Proctor, J. Forster, E. Perivolari, N. Podoliak, M. Sugden, R. Kirke, T. Regrettier, T. Heiser, M. Kaczmarek, and G. D'Alessandro, "Wide area mapping of liquid crystal devices with passive and active command layers," Appl. Opt. **56**(32), 9050–9056 (2017).
22. J. Bateman, M. Proctor, O. Buchnev, N. Podoliak, G. D'Alessandro, and M. Kaczmarek, "Voltage transfer function as an optical method to characterize electrical properties of liquid crystal devices," Opt. Lett. **39**(13), 3756 (2014).
23. N. Brouckaert, N. Podoliak, T. Orlova, D. Bankova, A. F. De Fazio, A. G. Kanaras, O. Hovorka, G. D'Alessandro, and M. Kaczmarek, "Nanoparticles induced property changes in nematic liquid crystals," Nanomaterials. **12**(3), 341 (2022).
24. D. Bilby, B. Frieberg, S. Kramadhati, P. Green, and J. Kim, "Design considerations for electrode buffer layer materials in polymer solar cells," ACS Appl. Mater. Interfaces **6**(17), 14964–14974 (2014).
25. Y. Zhou, C. Fuentes-Hernandez, and J. Shim, *et al.*, "A universal method to produce low–work function electrodes for organic electronics," Science. **336**(6079), 327–332 (2012).
26. S. Liu, D. Chen, X. Hu, Z. Xing, J. Wan, L. Zhang, L. Tan, W. Zhou, and Y. Chen, "Printable and large-area organic solar cells enabled by a ternary pseudo-planar heterojunction strategy," Adv. Funct. Mater. **30**(36), 2003223 (2020).
27. Q. An, F. Zhang, J. Zhang, W. Tang, Z. Deng, and B. Hu, "Versatile ternary organic solar cells: A critical review," Energy Environ. Sci. **9**(2), 281–322 (2016).
28. D. Bankova, N. Brouckaert, N. Podoliak, B. Beddoes, E. White, O. Buchnev, M. Kaczmarek, and G. D'Alessandro, "Characterization of optically thin cells and experimental liquid crystals," Appl. Opt. **61**(16), 4663 (2022).

Optical Materials EXPRESS

29. R. A. Street, K. W. Song, and J. E. Northrup, "Photoconductivity measurements of the electronic structure of organic solar cells," Phys. Rev. B **83**(16), 165207 (2011).
30. W. Tress, K. Leo, and M. Riede, "Optimum mobility, contact properties, and open-circuit voltage of organic solar cells: A drift-diffusion simulation study," Phys. Rev. B **85**(15), 155201 (2012).
31. D.-S. Seo, K. Araya, N. Yoshida, M. Nishikawa, Y. Yabe, and S. Kobayashi, "Effect of the polymer tilt angle for generation of pretilt angle in nematic liquid crystal on rubbed polyimide surfaces," Jpn. J. Appl. Phys. **34**(4B), L503 (1995).
32. S.-H. Paek and C. J. Durning, "A mechanistic picture of the effects of rubbing on polyimide surfaces and liquid crystal pretilt angles," J. Appl. Phys. **83**(3), 1270–1280 (1998).
33. L. Duan and A. Uddin, "Progress in stability of organic solar cells," Adv. Sci. **7**(11), 1903259 (2020).
34. P. Cheng and X. Zhan, "Stability of organic solar cells: challenges and strategies," Chem. Soc. Rev. **45**(9), 2544–2582 (2016).
35. Q. Burlingame, X. Huang, X. Liu, C. Jeong, C. Coburn, and S. R. Forrest, "Intrinsically stable organic solar cells under high-intensity illumination," Nature. **573**(7774), 394–397 (2019).
36. N. Brouckaert, "Nanoparticle induced property changes in nematic liquid crystals: supporting information," University of Southampton, 2023, https://doi.org/10.5258/SOTON/D2573

152.78.210.52 {ts '2023-07-25 10:45:31'}